Localized tissue mineralization regulated by bone remodelling: a computational approach

Marcelo Berli[1], Carlos Borau[2], Oscar Decco[1], George Adams[3], Richard B. Cook[4], José Manuel García Aznar[2], Peter Zioupos[3*]

[1] Facultad de Ingeniería, Universidad Nacional de Entre Ríos, Ruta 11, Km. 10, Oro Verde, Entre Ríos (3100), República Argentina.

[2] Departamento de Ingeniería Mecánica, Instituto de Investigación en Ingeniería de Aragón (I3A), Universidad de Zaragoza, 505018 Zaragoza, España

[3] Musculoskeletal & Medicolegal Research Group, Cranfield Forensic Institute, DA of the UK, Shrivenham, SN6 8LA, UK

[4] nCATS, University of Southampton, Highfield, Southampton, SO17 1BJ, UK

E-mail: p.zioupos@cranfield.ac.uk

Trabecular bone

Cortical bone

Abstract
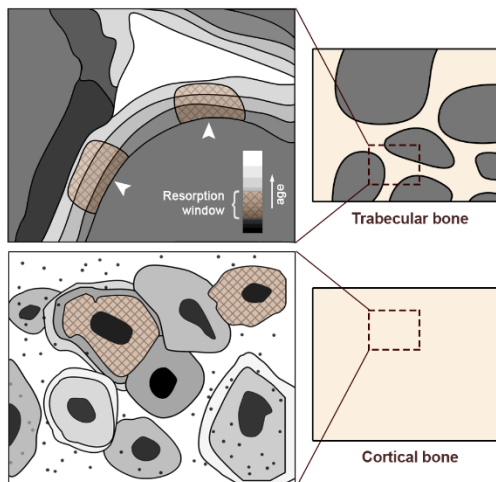
Bone is a living tissue whose main mechanical function is to provide stiffness, strength and protection to the body. Both stiffness and strength depend on the mineralization of the organic matrix, which is constantly being remodelled by the coordinated action of the bone multicellular units (BMUs). Due to the dynamics of both remodelling and mineralization, each sample of bone is composed of structural units (osteons in cortical and packets in cancellous bone) created at different times, therefore presenting different levels of mineral content. In this work, a computational model is used to understand the feedback between the remodelling and the mineralization processes under different load conditions and bone porosities. This model considers that osteoclasts primarily resorb those parts of bone closer to the surface, which are younger and less mineralized than older inner ones. Under equilibrium loads, results show that bone volumes with both the highest and the lowest levels of porosity (cancellous and cortical respectively) tend to develop higher levels of mineral content compared to volumes with intermediate porosity, thus presenting higher material densities. In good agreement with recent experimental measurements, a boomerang-like pattern emerges when plotting apparent density at the tissue level versus material density at the bone material level. Overload and disuse states are studied too, resulting in a translation of the apparent–material density curve. Numerical results are discussed pointing to potential clinical applications.

Keywords - bone remodelling; mineralization patterns; material density; BMU dynamics;

Introduction

Bone provides support and protection to the body, stores minerals and also enables mobility. Moreover, it is able to adapt, in a remodelling process, to local mechanical demands by distributing the tissue mass in response to a daily stress field [1–6]. This results in an heterogeneously mineralized material [7–10] showing bone structural units of different mineral contents. The mass distribution in the bone can be traced by the apparent density (ρ_{app}), which is the mineralized wet mass over the sample volume (V_t) and by its material density (ρ_{mat})

1

which is the mass over the volume occupied by the material itself (V_b). Therefore, the difference between these two densities is a geometrical one and is due to the presence of pores. Bone, therefore, regulates both its apparent and material densities to different degrees and different effects, to answer the loading demands placed upon it. After skeletal maturity is reached these processes continue to allow for damage repair and this results in a highly heterogeneous bone matrix which has been shown independently to affect bone strength [11]. It is widely accepted that as much as 70-80% of the variation in bone strength and stiffness can be explained by apparent density alone [12], while the remaining 20-30% is a corollary of the finer modulation of bone material density itself.

The relationship between ρ_{app} and ρ_{mat}, however, is elusive and not well-studied, but recently evidence has emerged that bone composition at tissue and material levels are linked as shown in the studies of Zioupos et al.[13]. These authors demonstrated a boomerang-like curvilinear pattern when plotting ρ_{app} vs ρ_{mat}, showing an inflection point that suggests a natural separation in the behaviour of cortical and cancellous bone. The consequences of this are twofold: at a fundamental level the results alluded to a profoundly different mineralizing pattern in cortical and cancellous bone, and at a practical level the findings may have implications for the accuracy of CT (Computer Tomography) and QCT (Quantitative Computer Tomography) scans used for diagnoses, or for assigning bone properties in micro-Finite Element simulations [13–19].

Modelling the bone remodelling process by computational methods was widely performed by two main approaches: macroscopic and microscopic. The main difference between these approaches lies in the scale of modelling which in turn allows describing with more or less detail the inner architecture of the bone. Macroscopic models [6,20–23] were extensively used due to the reduced computational cost, and although requiring an extensive mathematical formulation, allowed simulation of the remodelling process of an entire bone. In these models, the volumes occupied by both pores and bone itself at every location of the tissue are described by means of continuum (average) variables computed into a representative volume (V_t). Thus, the bone density at each V_t is actually the apparent density, which is the main variable that evolves in response to mechanical stimuli. In fact, the amount of tissue resorbed by osteoclasts and formed by osteoblasts are averaged quantities too, leading to an averaged bone volume, porosity and material density variations over time.

On the other hand, microscopic models [24–27] are able to describe in detail the internal architecture of the bone (microstructure), allowing thorough simulations of small bone samples but requiring higher computational costs. In these models, pores and bone tissue are treated as separate domains in the volume subject to simulation. Both osteoclasts and osteoblasts activities are explicitly modelled by predicting the effect of BMUs on bone surface over time, and the mineral evolution of every bone department can be traced not only in time but in space, so that the level of bone mineralization from the free surface to the core can be described.

The amount of surface that is available depends of course, on the cellularity (level of porosity of this biological material. Martin (1984) has presented the parabolic curve of the specific surface of bone throughout the whole range from very compact (cortical) to least dense (cancellous) at the bottom end and showed that the maximum area available, through which remodelling acts, shows a maximum somewhere in between for porosity levels in the [0.3-0.6] range. Recent actual measurements of this phenomenon by members of this group showed that modern CT scanners can segment and produce these curves easily for a range of bones sample and from different species [28] (see Fig 1).

Several computational models dealing with the mineralization process of bone can be found in the literature, each one of them making different assumptions. For instance, Martínez-Reina et al.[21] developed a macroscopic model assuming that osteoclasts digest bone independently on their location by using averaged volumes. That is to say, the surface of bone (younger) was resorbed in the same manner as its core (older). This approach allowed tracking different bone variables in time (volumes, densities, mineralization) but was unable to consider geometrical effects. In this sense, Hartman et al.[27] implemented a microscopic stochastic model in which bone resorption was performed only on the bone surface but in a random manner not controlled by mechanical stimulus. Although they obtained realistic mineral density distributions, they concluded that some discrepancies of their results with respect to experiments may arise from the fact that osteoclasts resorb preferentially low mineralized young bone at the bone surface, something for which they did not account for in their model. Indeed, measurements on cancellous bone made by Lukas et al.[29] confirmed that bone gets more mineralized toward the core of the trabecula, suggesting that osteoclasts have an effect that depends on the depth from the surface, as if they have a tendency to resorb low mineralized bone at the trabeculae's surface.
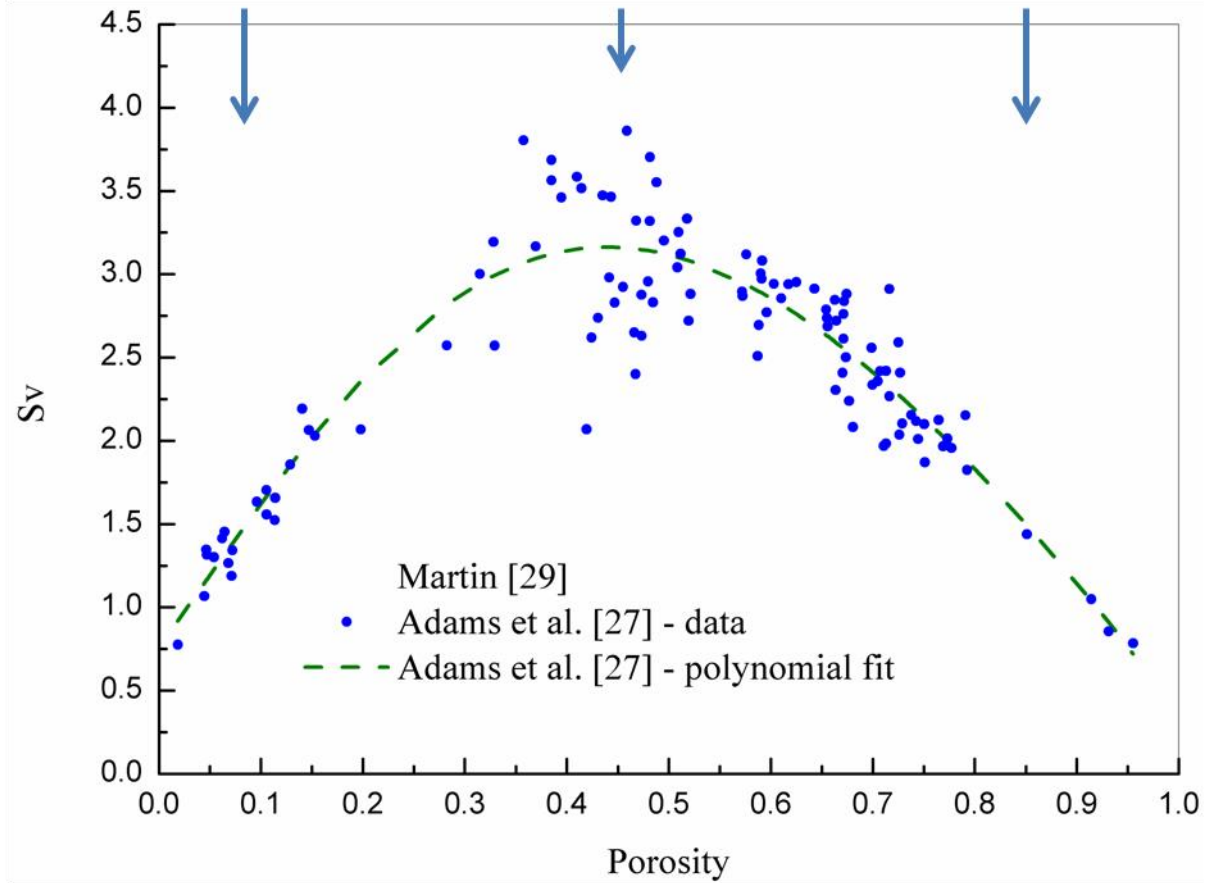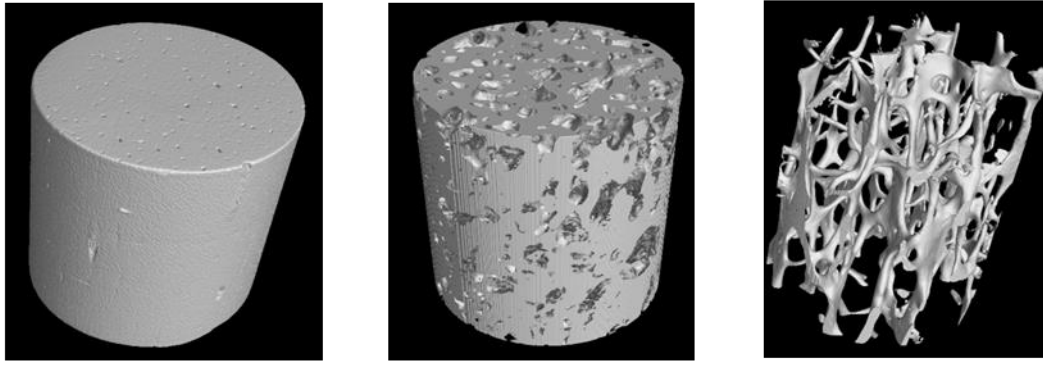
Fig 1: Specific Surface of bone as function of porosity (porosity = 1-BV/TV) from the analysis produced by Martin [30] (solid curve) and recent precise measurements by Adams et al.[28] (circles with a dashed line which is a fifth degree polynomial fit).

The present work is based on the fundamental approach that we established on macroscopic bone remodelling in the past [20,21], but now implementing a novel resorption strategy, which takes into account the observations that osteoclasts resorb preferably those parts of bone closer to the surface. This surface bone material is, in general, younger and less mineralized than the older inner one [29]. Further level of complexity is offered by exploring and considering the effects of different levels of initial bone densities, as well as external loads. The

model is quantitatively compared with the trends observed in the relationship between ρ_{app} and ρ_{mat} under equilibrium state as published in Zioupos et al.[13,31]. Computational bone remodelling models are difficult to corroborate as they lack data for validation at the microstructural level. In this respect, the macroscopic experimental data of Zioupos et al.[13], provides a rare opportunity to verify how the mineral content is laid down and re-distributed within the bone and the effects it has on its local and global mineralization patterns. The aim of this paper is to show how the mineral distribution in bone, as evident in the recent work [13] is linked to this resorption strategy. This macroscopic approach constitutes then, a starting point to elucidate the

3

biological mechanisms that could lead to the mineral distribution patterns observed in various other experimental observations.

Bone-remodelling computational model

The computational model proposed here is based on the same development steps introduced by García-Aznar et al.[20] and Martínez-Reina et al.[21]; these include a representative volume of bone, which is divided in different sub-volumes (solid matrix and pores) which evolve in time due to the action of the BMUs. BMUs constantly form and resorb bone activated by mechanical signals, which depend on external loads and material elasticity which in turn varies with bone mineralization (see Fig 2).

The present model incorporates a novel remodelling strategy based on the idea that osteoclasts tend to resorb newly formed bone closer to the surface, and not the highly mineralized one corresponding to the inner zones. Bone remodelling is a surface effect, very much a 2-D phenomenon which resembles diffusion in many of its details and its kinetics. This process and its implementation are detailed below; the main features that underpin the basic model are summarized in Appendix A.
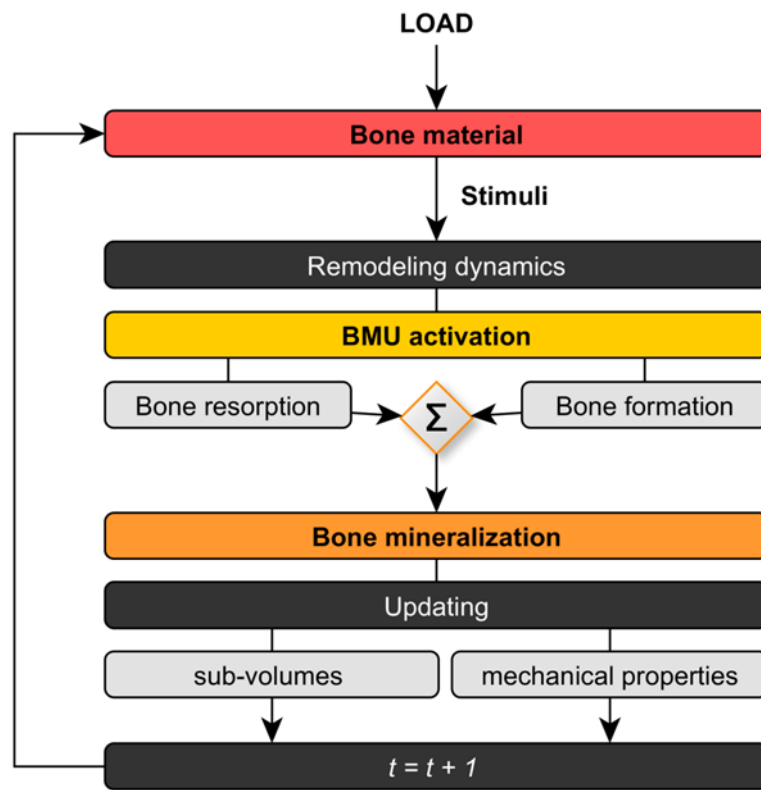

Fig 2: Simplified scheme of the bone-remodelling computational model [21]. Note that, for simplicity, some additional features like biological factors and damage dynamics are not shown in this flowchart to avoid confusion. Nonetheless, they are still present in the current approach.

Bone Composition

Bone tissue is composed by bone material and pores. The former is a composite of organic matrix (mainly collagen), water and mineral content, while the latter are filled with marrow, blood vessels and nerves. In this work, pores are regarded as void volumes, since the mechanical influence of the tissue inside is negligible with respect to the much stiffer matrix. Therefore, a reference bone tissue volume (V_t) can be divided into the bone material volume (V_b) and the volume of pores (V_p). The bone material volume is in turn composed by sub-volumes of mineral phase (V_m), organic phase (V_o), and water (V_w). Since bone is constantly being remodelled, every sub-volume evolves with time:

$$V_t = V_b(t) + V_p(t) = V_m(t) + V_o(t) + V_w(t) + V_p(t) \tag{1}$$

Note that V_b comprises volumes of portions of bone material formed at different times and therefore having a different mineralization level, as explained later.

To describe the temporal evolution of each sub-volume, the model defines the following ratios:

$$v_b(t) = \frac{V_b(t)}{V_t} \quad v_m(t) = \frac{V_m(t)}{V_b(t)}$$

$$v_o = \frac{V_o(t)}{V_b(t)} \quad v_w(t) = \frac{V_w(t)}{V_b(t)} \tag{2}$$

We consider v_o to have a constant value of 3/7 [21], and water is assumed to be replaced by mineral during the mineralization process. Hence, the next sum holds:

$$v_m(t) + v_o + v_w(t) = 1 \tag{3}$$

Having the evolution of every component of bone material volume fraction, we can compute the material density ρ_{mat}, which is actually the density of the solid bone matrix:

$$\rho_{mat}(t) = \rho_m v_m(t) + \rho_o v_o + \rho_w v_w(t) \tag{4}$$

Where densities of mineral, organic components and water are $\rho_m = 3.2 \text{ g}/\text{cm}^3$, $\rho_o = 1.1 \text{ g}/\text{cm}^3$ and $\rho_w = 1.0 \text{ g}/\text{cm}^3$ respectively [21]. This definition leads to a linear relationship between material density and mineral volume fraction. On the other hand, the apparent density ρ_{app}, the basic variable in most bone remodelling models [2,3,5,32,33], can be obtained through the bone material volume fraction and the material density:

$$\rho_{app}(t) = \rho_{mat}(t) v_b(t) \tag{5}$$

The ash fraction, which is defined as the ratio between the mineral mass and the dry mass (the sum of mineral and organic mass) can be expressed as follows:

$$\alpha = \frac{\rho_m v_m}{\rho_m v_m + \rho_o v_o} \tag{6}$$

In this way, the temporal evolution of $v_m(t)$ is linked to changes of α and vice versa.

Remodelling dynamics

According to our previous model [21], as time advances, certain parts of bone material are formed (v_f) while others are resorbed (v_r) therefore updating the bone material volume at each time step (v_b). Hence, the rate of change of the bone material volume fraction ($\dot{v}_b$), depends on the volume of bone material removed ($\dot{v}_r$) and formed ($\dot{v}_f$) per unit time, by all BMUs active at time t. Therefore $\dot{v}_b(t) = \dot{v}_f(t) - \dot{v}_r(t)$, with:

$$\dot{v}_r(t) = \int_{t-T_R}^{t} \left(\int_{t'-\sigma_L}^{t'} \dot{N}_{BMU}(t'')dt'' \right) \frac{A_{BMU}}{T_R} f_c(t') v_{BMU} dt'' \tag{7}$$

$$\dot{v}_f(t) = \int_{t-T_R-T_I-T_F}^{t-T_R-T_I} \left(\int_{t'-\sigma_L}^{t'} \dot{N}_{BMU}(t'')dt'' \right) \frac{A_{BMU}}{T_R} f_b(t') v_{BMU} dt'' \tag{8}$$

where $\dot{N}_{BMU}$ stands for the number of BMUs activated per unit time and unit volume (whose calculation can be consulted in appendix A), v_{BMU} is the speed of BMU progress, T_R is resorption period (first period of BMU action due to osteoclasts activity) followed by a reversal time (T_I) after which deposition of bone is performed by osteoblasts during the formation period (T_f), and σ_L is the lifespan of BMU. On the other hand, f_c and f_b measure the osteoclast/osteoblast activities respectively. It is important to note that the ratio f_b / f_c follows a piece-wise linear model as a function of the unbalanced stimulus $\xi - \xi^*$, being ξ^* the reference stimulus (see [20]). If $\xi = \xi^*$, $f_b = f_c$, $\dot{v}_r(t) = \dot{v}_f(t)$ and $\dot{v}_b(t) = 0$ (equilibrium). For higher stimulus, $\xi > \xi^*$, $f_b > f_c$ and bone formation dominates (porosity decreases), while for disuse, $\xi < \xi^*$, $f_b < f_c$ and resorption dominates (porosity increases). Finally, A_{BMU} is the section of the material volume unit resorbed by osteoclasts and then filled by osteoblasts. Osteon cross section is considered for the assumed range of cortical bone ($v_b > 0.7$), while hemiosteon is considered for cancellous bone ($v_b < 0.3$) [20]. In the transition zone, where $0.3 < v_b < 0.7$, a linear approach of the BMU section A_{BMU} is assumed (Fig 3).
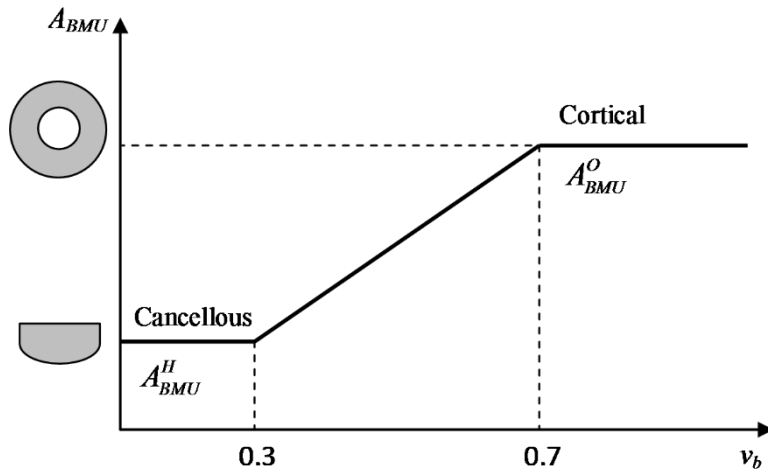

Fig 3. Cross section area (A_{BMU}) of the tissue volume unit that a single BMU remodels in cortical and cancellous bone as a function of bone material volume. For $v_b > 0.7$, osteonal cross section is considered while for $v_b < 0.3$, hemi-osteonal cross section is used instead. For bone material volume values between 0.3 and 0.7, a linear transition of cross section area is assumed.

Mineralization process

During the mineralization process, water is replaced by mineral and thus, the mineral content of every part of bone material increases with time [34]. As a result, the mineral volume of each part (v_m^*) evolves with time following the next assumed law (eq. 9), which distinguishes the three phases of mineralization: lag time where no deposition of mineral occurs, primary phase with a linear increase of mineral content, and the secondary phase with an exponentially decreasing rate [21]:

$$v_m^*(t) = \begin{cases} 0 & if\ t \le T_{nm} \\ v_m^{prim} \dfrac{t - T_{nm}}{T_{prim}} & if\ T_{nm} < t \le \left(T_{nm} + T_{prim}\right) \\ v_m^{max} - (v_m^{max} - v_m^{prim})e^{-\kappa_m(t - T_{prim} - T_{nm})} & if\ \left(t_{nm} + T_{prim}\right) > t \end{cases} \qquad (9)$$

where T_{nm} and T_{prim} are the length of the mineralization lag time and the primary phase respectively and κ_m is a parameter which measures the rate of mineral deposition in the secondary phase. v_m^{prim} is a constant representing the mineral volume ratio at the end of the primary phase($v_m^{prim} = 0.121$) and v_m^{max} corresponds to a volume ratio with the maximum calcium content ($v_m^{max} = 0.442$, 300 mg/g) [35].

To compute the mineral volume fraction of the whole bone (v_m), the mineralization law must be first established. The bone material volume fraction is composed by differential of bone created at day τ and still present at time t, this is:

$$v_b(t) = \int_{t-T_m^{Max}}^{t} \frac{dv_b(\tau)}{d\tau} d\tau \qquad (10)$$

where T_m^{Max} is the time required for a part of bone material to reach the maximum mineralization level. With every time increment, $\dot{v}_b(t)$ must be updated considering the amount of bone material formed ($dv_f(t) = \dot{v}_f(t)dt$) and resorbed ($dv_r(t) = \dot{v}_r(t)dt$). Normally, macroscopic bone remodelling laws do not take into account how and where this resorption occurs, but this is actually the cornerstone of the current approach. Our model assumes that osteoclasts tend to remove bone primarily from young surface areas, but only those presenting a minimum amount of mineral content, which excludes just newly created bone parts. Thus, we define a temporal window ($\Delta\tau = T_{sr}$) that includes those parts of bone candidates to be resorbed. If we call the lower bound of this window the non-mineralization time (T_{nm}), then the parts of bone material subject to be digested are those created in the time interval determined between T_{nm} and $T_{nm} + T_{sr}$ days ago. Following this, $v_m(t)$ can be computed as:

$$v_m(t) = \frac{1}{v_b(t)} \int_{t-T_m^{Max}}^{t} v_m^*(t-\tau) \frac{dv_b(\tau)}{d\tau} d\tau =$$

$$= \frac{1}{v_b(t)} \int_{t-T_m^{Max}}^{t} v_m^*(t-\tau) \frac{dv_f(\tau)}{d\tau} d\tau - \frac{1}{v_b(t)} \int_{t-T_{nm}-T_{sr}}^{t-T_{nm}} v_m^*(t-\tau) \frac{dv_r(\tau)}{d\tau} d\tau \qquad (11)$$

where $v_m^*(t-\tau)$ is the mineral volume fraction of each bone material part, calculated according to eq.9. The computational implementation the mineralization process is discussed in the following section.

Numerical implementation

The algorithm for bone remodelling was implemented in a user material subroutine (UMAT) linked to Abaqus. The main purpose of the model is to track the evolution of the different sub-volumes comprising a representative bone material volume fraction to study the mass distribution (densities) once the system reaches equilibrium. In order to take into account that the mineral content of every part of bone material depends on modelling history, the time at which such parts were formed is also stored and used in the equations. Fig 4 shows a representation of the bone as a mosaic of bone material parts with different mineral contents. It must be noted that the representation of the bone material by layers of increasing mineral content is based on the results of Lukas et al [29].

Since the mineralization could, theoretically, evolve indefinitely (see eq.9), we define a maximum mineralization time (T_m^{Max}) at which a certain volume is considered to reach v_m^{max}. In this way, we set a sufficiently large window data while keeping down the computational costs (array lengths) (see Table 1).

To account for the evolution of every part of bone material, the bone material volume fraction (v_b) is computationally implemented in an array containing the discrete portions of bone material volume fractions

$\Delta v_b(i)$, where every component of this array is the part of bone material formed *i* days ago and still present at time *t*. This array is homogeneously initialized in each simulation as:

$$\Delta v_b(i) = v_b^0 / T_m^{Max} \quad \text{for} \quad 0 < i \leq T_m^{Max} \tag{12}$$

where v_b^0 is the initial bone material volume fraction considered in each computation, ranging from 0.2 (cancellous bone) to 0.94 (cortical). How each component of $\Delta v_b(i)$ is calculated and updated is explained below in this section and is the essential foundation of our model.

Firstly, from eq.11 we distinguish four temporal windows: 1) the old mineralized tissue (formed between $T_{sr} + T_{nm}$ and T_m^{Max} days ago), far from the pore surface, 2) the younger bone material that is more likely to be resorbed (formed between T_{nm} and $T_{sr} + T_{nm}$ days ago), 3) the recently created bone material that lacks mineral content and is assumed to be ignored by the osteoclasts (formed from the current day to T_{nm} days ago) and 4) the recent bone material added at present time *t* due to osteoblasts activity. Hence, considering a computational time step of 1 day (i.e. $\Delta t = 1$ day), the bone volume fraction at each step is computed following eq.13:

$$v_b(t) = \overset{1)}{\sum_{i=T_{nm}+T_{sr}}^{T_m^{Max}} \Delta v_b(i)} + \overset{2)}{\sum_{i=T_{nm}}^{T_{nm}+T_{sr}-1} [\Delta v_b(i) - \Delta v_r(i)]} + \overset{3)}{\sum_{i=1}^{T_{nm}-1} \Delta v_b(i)} + \overset{4)}{\Delta v_f(t)} \tag{13}$$

where $\Delta v_r(i)$ is the array containing the portions to be removed from the parts of bone material formed *i* days ago, whose summation must fulfil that:

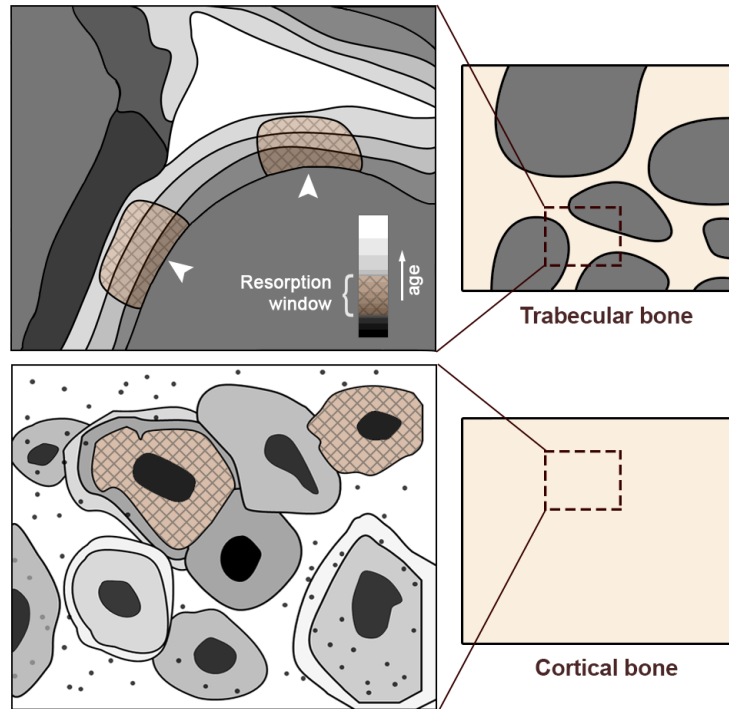$$\sum_{i=T_{nm}}^{T_{nm}+T_{sr}-1} \Delta v_r(i) = \dot{v}_r(t)\Delta t \tag{14}$$

Fig 4: Plot representing a reference bone volume (right) formed by solid matrix and pores. A magnifying box honing in on specific trabeculae (left) shows a mosaic of tissue structural units presenting a distribution of mineral content depending on bone age (grayscale, darker means younger and less mineralized). Since resorption is assumed to be performed preferably at the bone surface, a resorption temporal window is defined (shaded areas with stripes). The organization of the trabeculae in layers with growing mineral content is based on results by Lukas et al.[29]. Also, there is experimental evidence of the layer-like organization in compact bone as can be seen in the work by Boivin et al.[36]

It is worth noting that we assume that the volume to be resorbed is uniformly distributed along its i components, which means that the amount of bone material resorbed at time t takes the same number of parts from different ages along the resorption window ($\Delta v_r(i) = \dot{v}_r(t)\Delta t / T_{sr}$). It is also important the fact that in case that there is not enough bone material of a certain age to be removed, the resorption spreads to older parts of bone material, which is especially relevant in cases of disuse where $\dot{v}_r > \dot{v}_f$. This process is schematized in Fig 5.
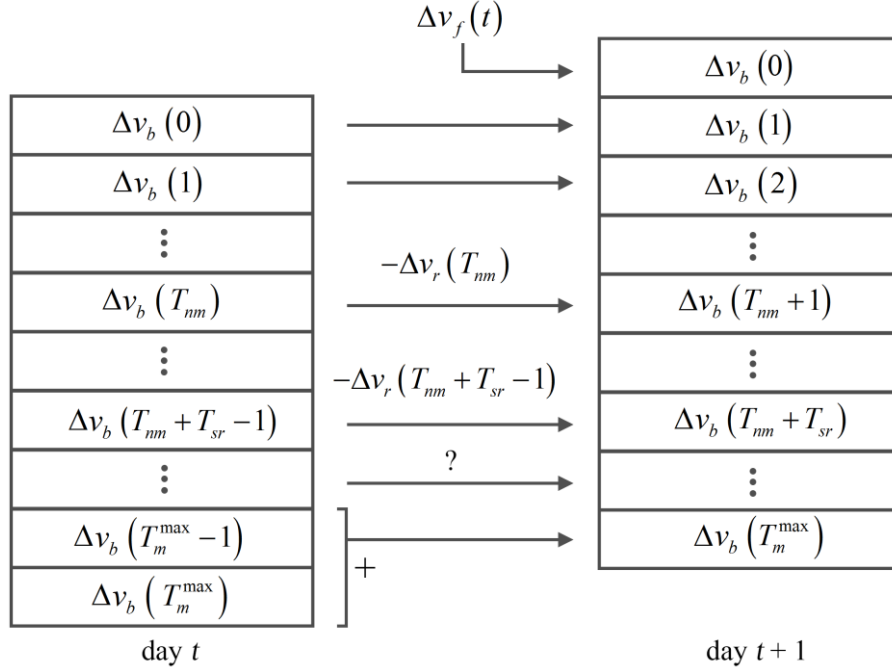

Fig 5: Updating scheme for the bone volume fraction array (Δv_b) of length ($T_m^{Max}+1$). The resorption starts on those components between T_{nm} and $T_{nm} + T_{sr} - 1$ positions. Note that if the values stored in such positions are not enough to fulfil the resorption rate at a specific time, further components are removed until the corresponding amount of bone is resorbed (question mark). Bone material surpassing the maximum mineralization time (T_m^{max}) is stored at the last position of the array to minimize computational costs.

Importantly, to account for the osteoclast population (and hence BMU activity) depending on the type of bone, we assume that the resorption window size varies proportionally to the available bone material specific surface (S_v), therefore depending on porosity ($p = 1 - v_b$) in a curvilinear parabolic fashion [28, 30]:

$$T_{sr} = \kappa_{sr} S_v = \kappa_{sr}\left(28.76 p^5 - 101.4 p^4 + 133.96 p^3 - 93.94 p^2 + 32.26 p\right) \tag{15}$$

where κ_{sr} is a scaling parameter to control the window resorption size. In this way, bone with very high or very low porosity (less surface area) is assigned smaller resorption windows compared to bone of intermediate porosity. Consequently, this fact alters the outcome of the mineralization process, because, and over a period of time, inner unresorbed parts of bone material with very low/high porosity keep on increasing their mineral content compared to bone in the transition from cancellous to cortical bone.

Once v_b is updated following the scheme shown in Fig 5, the new fraction of mineralized bone can be computed as follows:

$$v_m(t) = \frac{1}{v_b(t)} \sum_{i=0}^{T_m^{max}} \Delta v_b(i) v_m^*(i) \tag{16}$$

9

Consequently, v_w can be isolated and therefore ρ_{mat} and ρ_{app} can be obtained from equations 3 to 5. Further details about the mechanical problem and the computation of the stimulus driving the bone formation/resorption can be found in Supporting Info S1 Text.

Table 1: Parameters used in the simulations, extracted from [21]

Parameter		Reference	Range
General parameters			
A_{BMU}^{O}	Cortical A_{BMU}	4.3x10^{-3} mm^2	
A_{BMU}^{H}	Cancellous A_{BMU}	1.9x10^{-3} mm^2	
f_c	Measurement of osteoclast activity	1.0	
f_b / f_c	Balance between osteoblasts and osteoblasts activity.	1.0	0.95 – 1.05
ξ^*	Reference stimulus	0.00025	0.0-0.0005
V	Poisson coefficient	0.3	
v_o	Specific volume of organic phase	3/7	
ρ_m	Density of mineral phase	3.2 g/cm^3	
ρ_o	Density of organic phase	1.1 g/cm^3	
ρ_w	Density of water	1.0 g/cm^3	
Time spams in BMU activity			
T_r	Resorption period	24 days	
T_l	Reversal period	8 days	
T_f	Formation period	64 days	
v_{BMU}	Speed of BMU progress	0.04 mm/day	
σ_L	Lifespan of BMU	100 days	
Mineralization			
T_{nm}	Mineralization lag time	12 days	
T_{prim}	Length of primary phase	10 days	
T_m^{Max}	Time to reach the maximum mineral level	4000 days	
v_m^{prim}	v_m at the end of primary phase	0.121	
v_m^{max}	Maximal mineral specific volume	0.442	
κ_m	Rate of secondary phase	0.0005	
κ_{sr}	Scaling parameter controlling the size of the resorption window	200 days	150-250

Results and discussion

In order to test the impact of this bone's resorption hypothesis we examine the values that it gives us for material and apparent densities (ρ_{mat}, ρ_{app}) after a period of more than 20 years, having several initial bone material volume ratios, and different load cases. In particular, we explore the evolution of bone material with v_b^0 ranging from 0.2 to 0.94 and three levels of external load, namely: $\xi = \xi^*$ (equilibrium), $\xi = 0$ (disuse) and $\xi = 2\xi^*$ (overload). To facilitate the discussion, we will differentiate between three zones depending on the initial bone volume (v_b^0): (i) cancellous ($v_b^0 < 0.3$); (ii) transition ($0.3 < v_b^0 < 0.7$) and (iii) cortical ($v_b^0 > 0.7$).

Resorption dynamics regulates bone mineral distribution

Although it is well known that osteoclasts remove bone starting from the surface, how this phenomenon regulates bone mineralization is not completely understood. In this section, three different ways of resorption are tested, and the resulting material and apparent densities (ρ_{mat}, ρ_{app}) are compared with experimental measurements. In case-1, we use the assumptions from the previous model [21], in which osteoclast resorption is homogeneously distributed and independent of the bone level of mineralization (or equivalently, age). In case-2, osteoclasts are allowed to remove only the newly formed and poorly mineralized -bone material. In case-3, resorption is performed in the way proposed in this work, that is, being limited to a temporal window covering from recently, but not just newly created tissue, to those parts of bone material with an intermediate level of mineralization (formed between T_{nm} and $T_{sr} + T_{nm}$ days ago). To analyse the effect of the resorption window size (T_{sr}), different values of κ_{sr} are explored (see eq.15). All simulations in this section are performed under an equilibrium load $\xi = \xi^*$.

Fig 6 shows the simulated results superimposed to experimental measurements from [13]. In case-1 (dashed line with circles) all points fall at the left and outside of the measurements area, that is, the bone material presents lower ρ_{mat} than the experiments for all conditions (regardless of the initial v_b^0). This is due to the process being averaged over the complete bone material volume. Since the osteoclasts are able to reach the core of the bone material volume where those bone structural unit with the highest mineral content reside, the model predicts a lower mineralized tissue compared to the experimental data. Case-2 (dotted line with stars) represents the completely opposite idea: only those surface layers recently formed can be removed, so that the inner bone material remains unaltered and therefore has more time to reach higher mineralization levels. This hypothesis is too drastic and after a certain time, all the material is fully mineralized. This assumption yields a constant ρ_{mat} value regardless of the value of ρ_{app} (resulting in a vertical line) and predicts higher material densities for all the studied cases (right side of measurements data). These results, together with those from case-1, suggest that some hypothesis in between, like that proposed in case-3, might be adequate to match the experiments. In fact, results confirm an excellent agreement between the simulations from case-3 (solid lines with different markers) and the experimental measurements. Lower values of κ_{sr} lead to higher mineralization levels (higher ρ_{mat}) while higher values of κ_{sr} produce low mineralized bones. Thus, varying κ_{sr} allows a gradual shifting of the curves to the desired levels of densities. Note that if κ_{sr} was big enough to make T_{sr} as large as T_m^{Max} (the length of the array storing the history of bone material volumes), case-3 would be equivalent to case-1, since all the bone material would be subject to resorption regardless of its age and mineralization level.

In all cases, for all the values of κ_{sr} studied, the $\rho_{mat} - \rho_{app}$ curves show a boomerang-like pattern as that shown by Zioupos et al.[13]. This shape can be explained by the model assumptions themselves. Based on the model predictions, the adaptation of osteoclasts activity seems to depend on the available surface and therefore on porosity (or equivalently on v_b). Both cortical and cancellous bones (presenting lowest and highest porosities respectively), have small available surfaces so that the resorption concentrates on few portions of bone, which are constantly being renewed, while the inner parts keep mineralizing. This results in bones with very high ρ_{mat} and very high/low ρ_{app} (cortical/cancellous) which form the two tale ends of the boomerang pattern. On the other hand, bones with porosities in the transition zone ($0.3 < v_b^0 < 0.7$) have higher available surfaces so that the resorption reaches portions of bone with several levels of mineralization. This decreases the overall mineral content and thus forms the "nose" of the boomerang.

It is worth making here a comment on the absolute values of material density (ρ_{mat}). These at the peak of the curve at their lowest show values in the range of [1.5-1.7] g/cm³, which perhaps appear too low when according to Martin [30] osteoid has a density of 1.41 g/cm³ and fully mineralized bone has a density of 2.31 g/cm³. However, these (ρ_{mat}) were produced by the Archimedes suspension technique for measuring material density and this method thresholds everything that has a density higher than the suspending medium (1 g/cm³ for water). For Archimedes 'osteoid' starts at the collagen level (density of about 1.06 g/cm³ or thereabouts) and

everything above that is 'bone'. Radiographers and all other researchers define bone where mineral deposition has started and has actually taken place in a noticeable way. This indeed is for densities of 1.41 g/cm^3 and above, with some micro-CT scanners thresholding bone by default at 1.3 g/cm^3. Hence in reality Archimedes encompasses a broader range of 'bone' than any radiographic perception of this tissue.
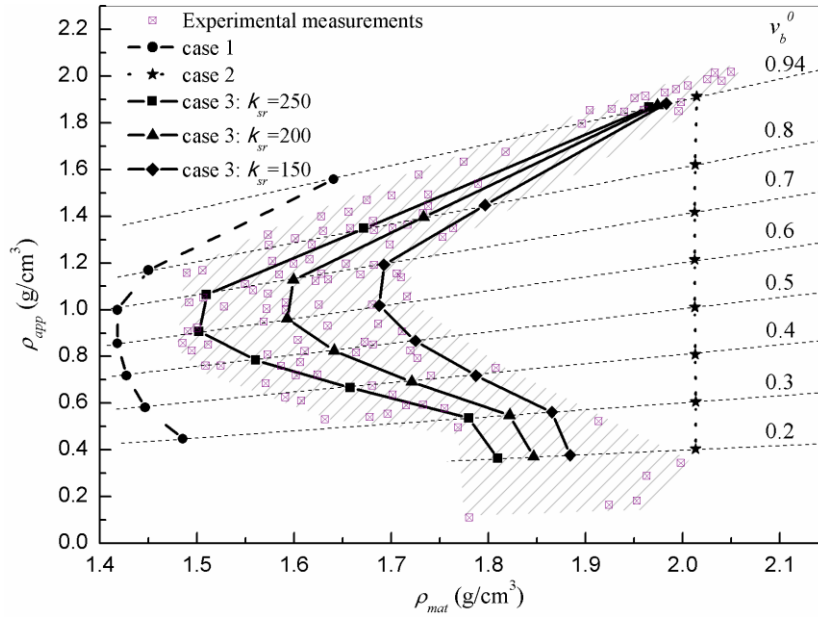

Fig 6. Tissue density (ρ_{mat}) vs apparent density (ρ_{app}) of bone for different temporal resorption conditions (initial bone volumes v_b^0 ranging from 0.2 to 0.94) superimposed with experimental measurements [13]. The plot presents the values at equilibrium state ($\xi = \xi^*$, t = 8000 days). Case-1 (dashed line with circles): resorption of bone is independent on temporal history and it is averaged through all the volume, including the most mineralized sub-volumes. This leads overall to the lowest material tissue densities for all the starting conditions we examine. Case-2 (dotted line with stars): resorption is only allowed to happen at the newly created bone, collapsing the curve to a vertical line where all bone volume is fully mineralized regardless v_b^0. Case-3: resorption is limited to temporal windows (bone parts created between T_{nm} and $T_{sr} + T_{nm}$ days ago), with three values of K_{sr}: 150 (solid line with diamonds), 200 (solid line with triangles) and 250 (solid dashed line with squares). The introduction of the hypothesis that resorption applies not just on newly created bone compartments but to recently formed bone up to 250 days, shifts the curves producing an envelope which practically covers the complete experimentally observed data set of points (cross-square dots).

It is worth mentioning that some curve shifting could also be achieved by adding the impact of the residual fat that could affect experimental measurements of densities as was pointed out by Schileo et al.[37]. However, the boomerang-like pattern will still appear since it depends on the resorption kinetics and not on the actual density values, as was predicted by Zioupos et al.[31]. Therefore, although the precise location of the boomerang curve may be disputed, its very shape is undeniable. On the other hand, care must also be taken in the definition of densities when analysing the results. For instance, if the material density is replaced by the ash density (ρ_{ash}) defined as the density of the mineral mass ($\rho_m V_m$) divided by the total bone tissue volume (V_t), a near monotonic trend of the ρ_{mat} vs ρ_{ash} relationship is obtained, which is in accordance with the experimental measurements by Schileo et al.et al.[38] (S1 Fig) .

External loads determine bone formation and mineralization

The very essence of mechanobiology is the response of tissues to external mechanical stimuli. So far, the effects of resorption dynamics have been explained under a specific load condition of $\xi = \xi^*$ (equilibrium). In this

section, we compare such effects with those produced by two diametrically opposed cases: overload ($\xi = 2\xi^*$) and disuse ($\xi = 0$). Overload is related to bone material changes during intense activity, whereas disuse is associated to prostration, microgravity and sedentary lifestyle, among others.

As shown in Fig 7A, overload leads to an enhanced bone material formation, especially relevant during the first 200 days, until the steady state (equilibrium) is reached after 1000 days. This net formation has a direct effect on mineralization since the inner parts are less likely to be resorbed and therefore their mineral content rises in time. This results in a lateral shift of the $\rho_{mat} - \rho_{app}$ curve towards overall higher material densities (right). This shift is greater at the transition zone where the bone kinetics is more intense (greater specific surface) and rapidly reduces in the cortical one. The observed shift has two corollaries: bone would appear to become more uniform in material density values and would also be perceived to be reinforced to support higher loads as has been demonstrated in various experiments [39,40].

By contrast, disuse cancels the inhibitory signal leading to an enhanced BMU activity which in turn creates an imbalance that greatly favours osteoclasts. The higher resorption activity leads to a dramatic reduction of bone volume (mainly in cortical bones) allowing osteoclasts to resorb greater amounts of high mineralized bone material and therefore substantially decreasing ρ_{mat}, which is in agreement with the experimental observations from [41]. Hence, all the points on the densities curve trajectory move to the left of the equilibrium case towards zones of less dense tissue (Fig 7B).
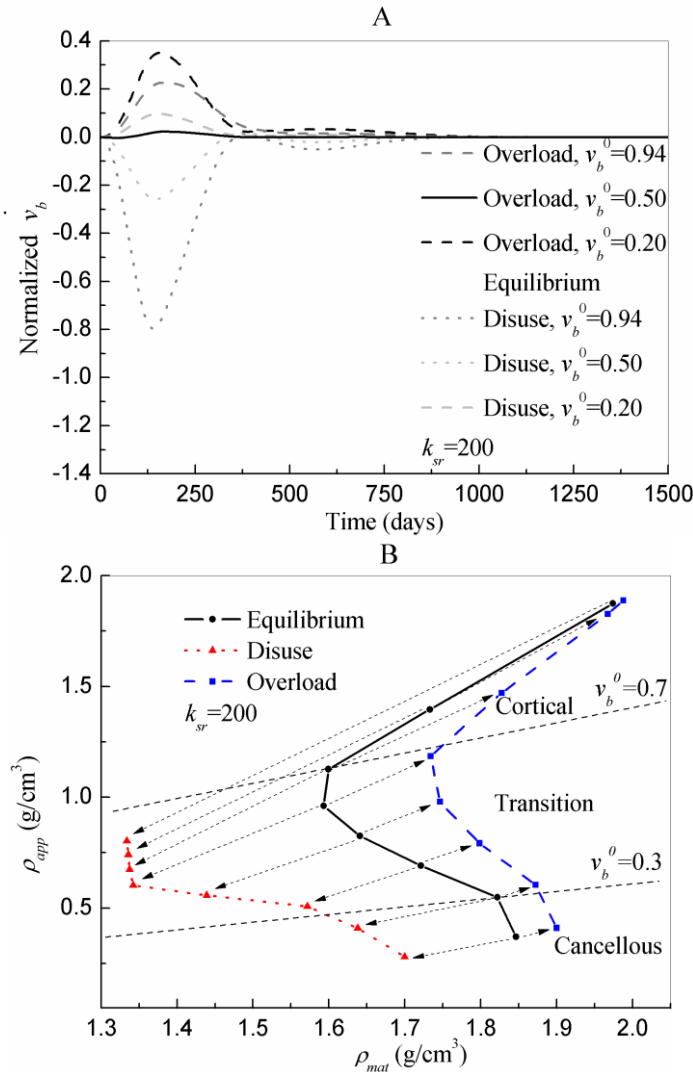

Fig 7: (A) Normalized bone volume formation rate for different load conditions (ξ applied uniaxial) and initial bone volumes (v_b^0). A parameter of resorption value of κ_{sr} = 200 was used in all the cases. Equilibrium ($\xi = \xi^*$, solid line): the amount of bone formed is the same as that of resorbed, leading to $\dot{v}_b = 0$ with only small oscillations during the first 400 days. Disuse ($\xi = 0$, dotted lines): the amount of bone resorbed is much higher

than bone being formed, leading to negative $\dot{v}_b$ until reaching equilibrium($\dot{v}_b = 0$) after about 1000 days. Overload ($\xi = 2\xi^*$, dashed lines): the amount of bone formed is higher than bone being resorbed, leading to positive $\dot{v}_b$ until reaching equilibrium ($\dot{v}_b = 0$) after about 1000 days. In both cases, the impact is especially relevant during the first 200 days in which the bone composition exhibits strong variations. After reaching a minimum/maximum, the effect gradually disappears, with small oscillations until equilibrium. (B) Tissue density (ρ_{mat}) vs apparent density (ρ_{app}) of bone for different load conditions (ξ Pa applied uniaxial). Arrows show translation of points with the same initial bone volume(v_b) from the equilibrium case (solid line with circles) to disuse or overload. In disuse (dotted line with triangles), both ρ_{mat} and ρ_{app} are greatly reduced compared to the equilibrium case. In the case of overload (dashed line with squares), ρ_{app} is mainly conserved, whereas ρ_{mat} is increased especially in the transition zone $(0.3 < v_b < 0.7)$

It must be noted that, under the almost fictitious extreme condition of complete disuse, "non-needed" bone is totally resorbed so that the cortical zone disappears. In this situation, the most mineralized bone material would be located in the trabecular zone. In turn, this means that physiologically, bone subjected to a long period of disuse would become so fragile that return to normal activities should be accomplished gradually and at pace dictated by the strength of the material. Although in reality this is not expected to happen throughout the whole bone, this phenomenon has been observed around implants supporting most of the load [42].

Conclusions

Understanding the full gamut of effects that govern bone formation and resorption, and being able firstly to handle the various factors and secondly to predict likely outcomes via a comprehensive model is a long term goal for bone mechanobiology [43-46]. The present work provides a novel paradigm in this quest by formulating our basic understanding of the material on some new basic assumptions on the spatial and temporal process of bone mineralisation in-situ and then validating it against some very recent extraordinary observations on the way bone densities behave locally and globally across the full range of bone volumes from cortical to cancellous [13,31]. The model was based on the earlier work by [20,21] and introduces a novel mathematical scheme implementing the bone formation/resorption cycle. Numerical predictions of this computational approach for the remodelling process are notoriously difficult to validate because the observations on determination of the spatial distribution of mineral content in the bone are, by and large, qualitative in their nature deriving from microscopy studies. However, the data presented by Zioupos et al.[13,31], on the macroscopic relationship between apparent density ρ_{app} (at tissue level) and material density ρ_{mat} (at material level) is truly quantitative and allows for this, so elusive, validation of the model.

Model predictions suggest a strong relationship between remodelling dynamics and the boomerang-like pattern of the $\rho_{app} - \rho_{mat}$ curve, with osteoclasts playing a key role in determining the mineral distribution in bone. Their activity has been linked to the available surface (remodelling is a 2-D effect driven and mediated through an active surface area) and therefore to porosity because the surface density of a cellular solid goes up and down with the overall porosity. In this sense, the model further stipulates that bone resorption happens preferentially on the younger low mineralized tissue, but after a minimal amount of mineral is reached. A geometric effect in the sense of depth from the free surface is also implicitly part of the formulation because newly formed less mineralised bone is more towards the surface with more mature and mineralised bone buried deep in the inner cores of the trabeculae. A suitable choice of the resorption window allows achieving accurate computational predictions and permits the adaptation of the model to account for the variability of the experimental data.

Mechanical loading also plays its part in determining the mineral distribution through the bone structure. Overload enhances bone formation, reinforcing the bone to support higher loads. Bone volume is increased at the surface so that the inner tissue increases even more its mineral levels, leading to higher ρ_{mat} compared to the equilibrium. It must be clarified that the selected load for this case($\xi = 2\xi^*$) is high enough to produce bone changes, but low enough to avoid damage, whose implications are out of the scope of the present work.

On the other hand, disuse leads to drastic reductions of both ρ_{mat} and ρ_{app}, completely eliminating the cortical zone. Osteoclasts remove the surplus of tissue leading to lighter but fragile bones.

In summary, the present study presents a paradigm shift offering new ways forward in the design of strategies of bone remodelling models to obtain more accurate bone structure predictions. The principal limitation of the present model is that it is analytical and so, the numerical results correspond to a macroscopic continuum model of bone that considers the distribution of the tissue in time but is averaged in space. Although we manage to capture some indirect geometrical effects through the resorption window strategy, a model of bone remodelling in 3-D, one that is capable of reproducing the specific geometry of bone trabeculae (e.g. a finite element approach) could refine these results by truly illustrating them in 3D space, thus becoming an important step forward to a better understanding of remodelling bone dynamics.

Ethics

The density data on which this model is based was produced in previous papers in the Biomechanics laboratories of the Cranfield Forensic Institute, from specimens from an Asian Elephant which died from natural causes and provided by Whipsnade Zoo through Prof. J Hutchinson of the Royal Veterinary College of Univ. London. There was no ethical issues because the animal involved died for reasons entirely unrelated to the study and was donated without restrictions on its research usage to John Hutchinson at the RVC. As the animal remained within the UK/EU there were no IUCN Endangered species status restrictions either on transport of its tissues for such research, and of course, there were no welfare/suffering issues as the animal did not become part of the research project until well after its untimely demise.

Data accessibility

The data underpinning this article is available through the Cranfield University CORD data depository and preservation (https: //cranfield.figshare.com) at https://doi.org/10.17862/cranfield.rd.4725784.

Competing interests

All authors of this ms declare that they have no competing interests.

Financial Disclosure

Authors' contributions

MB, CB, OD, JMGA, PZ were responsible for conceptualization; MB, CB, OD, JMGA formal analysis; MB, CB, JMGA, PZ funding acquisition; GA, RBC, PZ investigation; MB, CB, OD, CB, JMGA methodology; JMGA, PZ project administration; JMGA, PZ supervision; MB, CB validation; MB, CB, OD, JMGA visualization; MB, CB, PZ writing up; PZ reviewing.

References

1.   García JM, Doblaré M, Cegoñino J. Bone remodelling simulation: a tool for implant design. Comput Mater Sci. 2002; 25: 100–114. doi: 10.1016/S0927-0256(02)00254-9

2.   Doblaré M, García JM. Application of an anisotropic bone-remodelling model based on a damage-repair theory to the analysis of the proximal femur before and after total hip replacement. J Biomech. 2001; 34: 1157–1170. doi: 10.1016/S0021-9290(01)00069-0

3.   Doblaré M, García JM. Anisotropic bone remodelling model based on a continuum damage-repair theory. J Biomech. 2002; 35: 1–17. doi: 10.1016/S0021-9290(01)00178-6

4.   Reina JM, García-Aznar JM, Domínguez J, Doblaré M. Numerical estimation of bone density and elastic constants distribution in a human mandible. J Biomech. 2007; 40: 828–836. doi: 10.1016/j.jbiomech.2006.03.007

5.   Beaupré GS, Orr TE, Carter DR. An approach for time-dependent bone modeling and remodeling-application: a preliminary remodeling simulation. J Orthop Res. 1990; 8: 662–70. doi: 10.1002/jor.1100080507

6.   Huiskes R, Ruimerman R, van Lenthe GH, Janssen JD. No Title. Nature. 2000; 405: 704–706. doi: 10.1038/35015116

7.   Roschger P, Gupta HS, Berzlanovich A, Ittner G, Dempster DW, Fratzl P, et al. Constant mineralization density distribution in cancellous human bone. Bone 2003; 32: 316–323. doi: 10.1016/S8756-3282(02)00973-0

8.   Roschger P, Paschalis EP, Fratzl P, Klaushofer K. Bone mineralization density distribution in health and disease. Bone 2008; 42: 456–466. doi: 10.1016/j.bone.2007.10.021

9.   Koehne T, Vettorazzi E, Küsters N, Lüneburg R, Kahl-nieke B, Püschel K, et al. Trends in trabecular architecture and bone mineral density distribution in 152 individuals aged 30 – 90 years. Bone 2014; 66: 31–38. doi: 10.1016/j.bone.2014.05.010

10.   Sansalone V, Bousson V, Naili S, Bergot C, Peyrin F, Laredo JD, et al. Anatomical distribution of the degree of mineralization of bone tissue in human femoral neck : Impact on biomechanical properties. Bone 2012; 50: 876–884. doi: 10.1016/j.bone.2011.12.020

11.   Zioupos P, Gresle M, Winwood K Fatigue strength of human cortical bone: age physical and material heterogeneity effects. Journal of Biomedical Materials Research Part A, 2008; 86 (3): 627-636. doi:10.1002/jbm.a.31576

12.   Zioupos P, Aspden RM. Density, material-quality and quantity issues in OP cancellous bone. Proceedings Congress European Society Biomechanics-2000, 27-30 August 2000, Dublin, Ireland

13.   Zioupos P, Cook RB, Hutchinson JR. Some basic relationships between density values in cancellous and cortical bone. J Biomech. 2008; 41: 1961–1968. doi: 10.1016/j.jbiomech.2008.03.025

14.   Helgason B, Perilli E, Schileo E, Taddei F, Brynjólfsson S, Viceconti M. Mathematical relationships between bone density and mechanical properties: A literature review. Clin Biomech. 2008; 23: 135–146. doi: 10.1016/j.clinbiomech.2007.08.024

15.   Chen G, Schmutz B, Epari D, Rathnayaka K, Ibrahim S, Schuetz MA, et al. Short communication A new approach for assigning bone material properties from CT images into finite element models. J Biomech. 2010; 43: 1011–1015. doi: 10.1016/j.jbiomech.2009.10.040

16.   Schileo E, Taddei F, Cristofolini L, Viceconti M. Subject-specific finite element models implementing a maximum principal strain criterion are able to estimate failure risk and fracture location on human femurs tested in vitro. J Biomech. 2008; 41: 356–367. doi: 10.1016/j.jbiomech.2007.09.009

17.   Elsyad MA, Khirallah AS. Circumferential bone loss around splinted and nonsplinted immediately loaded implants retaining mandibular overdentures: A randomized controlled clinical trial using cone beam computed tomography. J Prosthet Dent. 2016; doi: 10.1016/j.prosdent.2016.03.005

18.   Oh TS, Park JS, Choi JW, Kwon SM, Koh KS. Risk factor analysis of bone resorption following secondary alveolar bone grafting using three-dimensional computed tomography. J Plast Reconstr Aesthetic Surg. 2016; 69: 487–492. doi: 10.1016/j.bjps.2015.11.002

19.   Roschger P, Paschalis EP, Fratzl P, Klaushofer K. Bone mineralization density distribution in health and disease. Bone 2008; 42: 456–466. doi: 10.1016/j.bone.2007.10.021

20.   García-Aznar JM, Rueberg T, Doblare M. A bone remodelling model coupling microdamage growth and repair by 3D BMU-activity. Biomech Model Mechanobiol. 2005; 4: 147–167. doi: 10.1007/s10237-005-0067-x

21.   Martínez-Reina J, García-Aznar JM, Domínguez J, Doblaré M. On the role of bone damage in calcium homeostasis. J Theor Biol. 2008; 254: 704–712. doi: 10.1016/j.jtbi.2008.06.007

22. Carter DR, Fyhrie DP, Whalen RT. Trabecular bone density and loading history: regulation of connective tissue biology by mechanical energy. J Biomech. 1987; 20: 785–94. Available: http://www.ncbi.nlm.nih.gov/pubmed/3654678

23. Martínez-Reina J, Reina I, Domínguez J, García-Aznar JM. A bone remodelling model including the effect of damage on the steering of BMUs. J Mech Behav Biomed Mater. 2014; 32: 99–112. doi: 10.1016/j.jmbbm.2013.12.025

24. Weinkamer R, Hartmann MA, Brechet Y, Fratzl P. Stochastic lattice model for bone remodeling and aging. Phys Rev Lett. 2004; 93: 228102. doi: 10.1103/PhysRevLett.93.228102

25. Ruimerman R, Hilbers P, van Rietbergen B, Huiskes R. A theoretical framework for strain-related trabecular bone maintenance and adaptation. J Biomech. 2005; 38: 931–41. doi: 10.1016/j.jbiomech.2004.03.037

26. van Oers RFM, Ruimerman R, Tanck E, Hilbers PAJ, Huiskes R. A unified theory for osteonal and hemi-osteonal remodeling. Bone. 2008; 42: 250–9. doi: 10.1016/j.bone.2007.10.009

27. Hartmann MA, Dunlop JWC, Bréchet YJM, Fratzl P, Weinkamer R. Trabecular bone remodelling simulated by a stochastic exchange of discrete bone packets from the surface. J Mech Behav Biomed Mater. 2011; 4: 879–887. doi: 10.1016/j.jmbbm.2011.03.005

28. Adams G, Cook R, Hutchinson J, Zioupos P. Bone surface distribution across a wide porosity range in mammalian bone tissue. 7th World Congress Biomechanics (WCB 2014) Proceedings of Meeting 6-11 July, 2014, Boston, MA, USA, ISBN:9781634393812

29. Lukas C, Ruffoni D, Lambers FM, Schulte FA, Kuhn G, Kollmannsberger P, et al. Mineralization kinetics in murine trabecular bone quanti fi ed by time-lapsed in vivo micro-computed tomography. Bone 2013; 56: 55–60. doi: 10.1016/j.bone.2013.05.005

30. Martin RB. Porosity and specific surface of bone. Crit Rev Biomed Eng. 1984; 10: 179–222. Available: http://www.ncbi.nlm.nih.gov/pubmed/6368124

31. Zioupos P, Cook RB, Hutchinson JR. More thoughts on the relationship between apparent and material densities in bone. J Biomech. 2009; 42: 794–5. doi: 10.1016/j.jbiomech.2009.01.014

32. Weinans H, Huiskes R, Grootenboer HJ. The behavior of adaptive bone-remodeling simulation models. J Biomech. 1992; 25: 1425–1441. doi: 10.1016/0021-9290(92)90056-7

33. Jacobs CR, Simo JC, Beaupre GS, Carter DR. Adaptive bone remodeling incorporating simultaneous density and anisotropy considerations. J Biomech. 1997; 30: 603–613. doi: 10.1016/S0021-9290(96)00189-3

34. Morin C, Hellmich C. Mineralization-driven bone tissue evolution follows from fluid-to-solid phase transformations in closed thermodynamic systems. J Theor Biol. 2013; 335: 185–197. doi: 10.1016/j.jtbi.2013.06.018

35. Currey JD. Tensile yield in compact bone is determined by strain, post-yield behaviour by mineral content. J Biomech. 2004; 37: 549–56. doi: 10.1016/j.jbiomech.2003.08.008

36. Boivin G, Bala Y, Doublier A, Farlay D, Ste-marie LG, Meunier PJ, et al. The role of mineralization and organic matrix in the microhardness of bone tissue from controls and osteoporotic patients. Bone, 2008; 43: 532–538. doi:10.1016/j.bone.2008.05.024

37. Schileo E, Taddei F, Baleani M. Letter to the Editor referring to the article "Some basic relationship between density values in cancellous bone and cortical bone" published on Journal of Biomechanics (volume 41, Issue 9, Pages 1961-8). J Biomech. 2009; 42: 793. doi: 10.1016/j.jbiomech.2009.01.013

38. Schileo E, Ara ED, Taddei F, Malandrino A, Schotkamp T, Ã MB, et al. An accurate estimation of bone density improves the accuracy of subject-specific finite element models. J Biomech 2008; 41: 2483–2491. doi: 10.1016/j.jbiomech.2008.05.017

39. Birkhold AI, Razi H, Weinkamer R, Duda GN, Checa S, Willie BM. Monitoring in vivo (re) modeling : A computational approach using 4D microCT data to quantify bone surface movements. Bone 2015; 75: 210–221. doi: 10.1016/j.bone.2015.02.027

40. Weatherholt AM, Fuchs RK, Warden SJ. Cortical and trabecular bone adaptation to incremental load magnitudes using the mouse tibial axial compression loading model. Bone 2013; 52: 372–379. doi: 10.1016/j.bone.2012.10.026

41. Grimm D, Grosse J, Wehland M, Mann V, Elin J, Sundaresan A, et al. The impact of microgravity on bone in humans. Bone 2016; 87: 44–56. doi: 10.1016/j.bone.2015.12.057

42. Tavakkoli P, Samiezadeh S, Bougherara H. Long-term response of femoral density to hip implant and bone fracture plate : Computational study using a mechano-biochemical model. Med Engng Phys. 2016; 38: 171–180. doi: 10.1016/j.medengphy.2015.11.013

43. Matsuo K, Irie N. Osteoclast–Osteoblast communication. Arch Biochem Biophys. 2008; 473: 201–209. doi:10.1016/j.abb.2008.03.027

44. Sims NA, Vrahnas C. Regulation of cortical and trabecular bone mass by communication between osteoblasts, osteocytes and osteoclasts. Arch Biochem Biophys. 2014; 561: 22–28. doi:10.1016/j.abb.2014.05.015

45. Martin R. Toward a unifying theory of bone remodeling. Bone 2000; 26: 1–6. doi:10.1016/S8756-3282(99)00241-0

46. Mikić B, Carter DR. Bone strain gage data and theoretical models of functional adaptation. J Biomech. 1995; 28: 465–469. doi:10.1016/0021-9290(94)00085-I

Supporting Information

S1 Fig. Apparent bone density vs ash density. Comparison of the model output to recent data in the literature. Measurements extracted from Schileo et al. [38] superimposed to numerical results derived from the present model for (κ_{sr} = 150). Note that the ash density is defined as the ratio of mineral mass to the reference bone volume

$$(\rho_m V_m / V_t).$$

S2 Fig. Results of the model by using the Specific Surface from Martin [30] (κ_{sr}^{M}) and from Adams et al.(2014) measurements (κ_{sr}^{AZ}), compared with other data from Zioupos et al.[13]. Derivation of different model outputs depending on different inputs for the bone surface density function. Note that the smaller specific surface from Adams et al.[28] implies narrower temporal windows of resorption and a lower osteoclasts activity, translating all points to the higher material density zone. However, the boomerang-like pattern still emerges in all these cases simply shifting it position to higher or lower density values. In order to match precisely the data with specific surface values from Adams et al.[28], a wider temporal window should be implemented, meaning that with a smaller specific surface, osteoclasts may reach the inner and more mineralized bone to achieve the agreement between measurements and model results.

S3 Fig. Histomorphometry of human elephant and human femoral cancellous samples in comparison. Plots of Tb.Th, Tb.N, Tb.Sp and BS/TV versus BV/TV. The histomorphometry of these two species is very similar and thus the full ranges of samples used here allowed us to build a more generic model. This model has been validated for the present elephant samples but can be finely tuned for human or other mammalian tissues by suitable adjustment of the various parameters.

S1 Text. Appendix to the main text describing the early evolution of the model

The evolution of bone volumes in time is governed by the Basic Multicellular Unit (BMU) activity, by resorbing bone by osteoclasts and depositing it by osteoblasts. Under normal conditions and health, bone resorption by osteoclasts is followed by osteoblastic bone formation, so that resorbed lacunae are filled to the original level by osteoblasts [43] and the bone remains with almost the same mass and structure [44]. If no regulation is exerted by osteocytes from bone matrix (inhibitory signal, s), it is believed that bone lining cells are inclined to activate BMU [45], depending on metabolic and biological factors (f_{bio}) and, of course, on the available free surface on which BMU may act (S_v). Thus, BMU activity is measured by its activation frequency, expressed as [20,21]:

$$\dot{N}_{BMU} = f_{bio} S_v \left(1-s\right) \qquad\qquad \text{eq S.1}$$

The inhibitory signal s from the osteocytic network follows here the theory proposed by Martin [45] and is defined as:

$$s = \frac{\xi}{\xi + c}(1-d)^a \qquad \text{eq S.2}$$

where a and c are constants extracted from Martinez-Reina et al [21] (see S1 Table).

Osteocytes sense not only mechanical stimulus (ξ), but also the appearance of micro cracks due to tissue damage (d). For the former, the stimulus is expressed as the daily strain history based on the strain level and the number of cycles, n_i, for each load case [46]:

$$\xi = \left(\sum_i n_i \bar{\varepsilon}_i^m\right)^{1/m} \qquad \text{eq S.3}$$

where the parameter m is taken to be 4 [46] and the effective strain, $\bar{\varepsilon}$ is defined as a function of the strain energy density (U), and the actual elastic modulus, E:

$$\bar{\varepsilon} = \sqrt{\frac{2U}{E}} \qquad \text{eq S.4}$$

Damage (d), the other variable sensed by osteocytes, is related to density microcracks and can be measured macroscopically. It is used in the isotropic theory of continuum damage mechanics [21]. Its values are restricted to the interval [0,1], with $d = 0$ corresponding to an undamaged state and $d = 1$ to local rupture situation. Following this theory, damage may also be correlated with the mechanical degradation or loss of stiffness, as:

$$d = 1 - \frac{E}{E_0} \qquad \text{eq S.5}$$

where E_0 is the elastic modulus of the bone in an ideal situation [21]. Development of the theory and detailed equations for damage and its evolution under compression or tension can be consulted in Martinez-Reina et al. [21].

The elastic modulus of the tissue evolves with the bone volume v_b and the ash α fractions, and is estimated by:

$$E(MPa) = 84370 v_b^{2.58} \alpha^{2.74}(1-d)$$

Finally the Poisson ratio is set to a constant value of $\nu = 0.3$ [20]

S1 Table. Values of the parameter of the model presented in supporting information

Parameter		Value
General parameters		
m	Weighting exponent	4
a	Damage activation exponent	40
c	Reference equilibrium stimulus	0.025
f_{bio}	Biological frequency factor	0.005
E_0	Elastic modulus of undamaged bone	84370 MPa
ν	Poisson ratio	0.3